ACS Catalysis

Research Article

pubs.acs.org/acscatalysis

A Density Functional Theory (DFT) Mechanistic Study of Gold(I)-Catalyzed Alkynylation of the Indole and Pyrrole Substrates, Using a Hypervalent Iodine Reagent

Alireza Ariafard*

Department of Chemistry, Faculty of Science, Central Tehran Branch, Islamic Azad University, Shahrak Gharb, Tehran, Iran
School of Chemistry, University of Tasmania, Private Bag 75, Hobart TAS 7001, Australia

Supporting Information

ABSTRACT: Density functional theory (DFT) was utilized to probe the mechanism of AuCl-catalyzed alkynylation of the indole and pyrrole substrates using a hypervalent iodine reagent ([(tri-*iso*-propysilyl)ethynyl]-1,2-benziodoxol-3(1*H*)-one (TIPS-EBX)). An unprecedented reaction mechanism was shown to be operative. In this mechanism, the catalytic reaction starts with coordination of the alkyne moiety of the iodine(III) reagent to the AuCl catalyst, followed by transfer of the alkynyl group from I^{III} to Au^{I}. The iodine(III) center was found to be capable of activating the alkyne triple bond more efficiently than the gold(I) center. The nucleophilic attack of the aromatic substrates on the I^{III}-activated alkyne gives a iodine(III) gold(I) vinyl complex. According to the calculations, this step was predicted to be the rate-determining step. Starting from the vinyl complex, the product is formed through the interaction of the occupied σ_{Au-C}-orbital with the vacant σ^*_{I-C}-orbital, followed by a very fast deprotonation reaction. This process that leads to the reduction of iodine(III) to iodine(I) occurs without protonation of the benzoate group of the iodine(III) moiety and with a small activation energy of 6.6 kcal/mol. It was concluded that the presence of the Au−C σ-bond at the β-position converts the vinyl group to a potent reductant. The regioselectivity for the catalytic C−H alkynylation of arenes is dictated by the stability of the vinyl complex. It was found that the cationic gold complexes such as PMe_3Au^+ are not effective catalysts for the alkynylation reaction, because they are strongly poisoned by coordination to the benzoate group of the iodine(III) reagent.

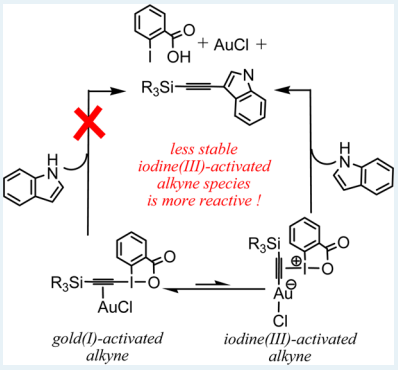

KEYWORDS: *gold, alkynylation, indole, pyrrole, hypervalent iodine reagent, density functional theory (DFT)*

INTRODUCTION

Transition-metal-catalyzed cross-coupling reactions have attracted considerable interest, because of their importance in synthesis and medicinal chemistry. In this regard, some research efforts have been focused on development of new synthetic methods for alkynylation of aromatic C−H bonds.[1] Recently, the hypervalent iodine reagents have been used to promote alkynylation of aromatic compounds using transition-metal catalysts.[2] For example, Waser and co-workers reported Au^{I}-catalyzed alkynylation of pyrroles and indoles using [(tri-*iso*-propysilyl)ethynyl]-1,2-benziodoxol-3(1*H*)-one (TIPS-EBX) (Scheme 1).[3] Through this methodology, many different alkynylated pyrroles and indoles were synthesized. Interestingly, the regioselectivity of this reaction was found to be strongly dependent on the identity of the aromatic substrate; the alkynylation for pyrroles occurs at C2 and for indoles at C3.

To account for the alkynylation reaction, three different mechanistic pathways have been proposed in the literature.[3,4] Scheme 2 shows the proposed possible pathways for indole alkynylation. Pathway (a) involves the nucleophilic addition of the indole at C^b of the Au^{I}-activated triple bond followed by proton transfer to the carboxylate group, giving gold vinyl intermediate **II**. This gold vinyl intermediate then undergoes the

Scheme 1. Alkynylation of Indoles and Pyrroles Using TIPS-EBX Catalyzed by AuCl

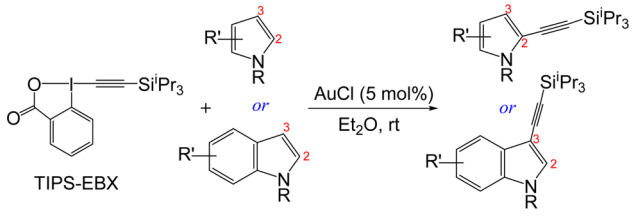

β-elimination to produce the final product (**prod**). In pathway (b), the intermediate **I** is trapped by nucleophilic addition of the indole at C^a, thereby giving intermediate **III** after deprotonation of indole. Starting from **III**, **prod** is formed via an α-elimination followed by a 1,2 shift rearrangement. The alkynylation reaction in pathway (c) proceeds via the oxidative addition of the C−I bond to Au^{I} to afford the Au^{III} intermediate **IV**. This intermediate

Received: May 5, 2014
Revised: July 13, 2014
Published: July 21, 2014

 © 2014 American Chemical Society

Scheme 2. Proposed Mechanisms for the Alkynylation of Indoles

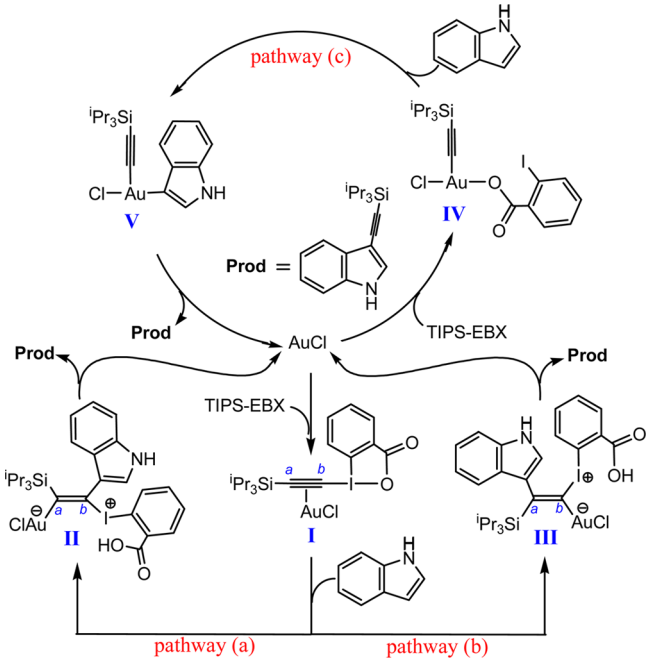

then reacts with the indole to give **V**, from which a C−C reductive elimination generates the final product.

The dilemma as to which catalytic cycle is responsible prompted us to employ density functional theory (DFT) to investigate this reaction in detail. Intriguingly, here, we show that an alternative mechanism in which the hypervalent iodine center operates as the Lewis acid for activating the alkyne is the most feasible. We believe that disentangling the mechanism of the alkynylation reaction can provide some insights into designing future reaction protocols.

COMPUTATIONAL DETAIL

Gaussian 09[5] was used to fully optimize all the structures reported in this paper at the B3LYP level of DFT[6] in Et_2O using the CPCM[7] solvation model. The effective-core potential of Hay and Wadt with a double-ξ valence basis set (LANL2DZ)[8] was chosen to describe Au and I. The 6-31G(d) basis set was used for other atoms.[9] Polarization functions were also added for Au (ξ_f = 1.050) and I (ξ_f = 0.289).[10] This basis set combination will be referred to as BS1. Frequency calculations were carried out at the same level of theory as those for the structural optimization. Transition structures were located using the Berny algorithm. Intrinsic reaction coordinate (IRC)[11] calculations were used to confirm the connectivity between transition structures and minima. To further refine the energies obtained from the B3LYP/BS1 calculations, we carried out single-point energy calculations for all of the structures with a larger basis set (BS2) in Et_2O using the CPCM solvation model at the B3LYP and M06[12] levels. BS2 utilizes the quadruple-ζ valence def2-QZVP basis set[13] on Au and I and the 6-311+G(2d,p) basis set on other atoms. We have used the potential and Gibbs free energies obtained from the M06/BS2//B3LYP/BS1 calculations in Et_2O throughout the paper, unless otherwise stated. Recent computational studies on organometallic reactions have shown that thermodynamic and kinetic results are predicted more accurately if the M06 functional is used instead of B3LYP.[12] The use of M06 can also be rationalized based on the fact that this functional estimates the van der Waals interactions more precisely.[14] These factors have prompted us to select this functional for all the single point calculations. The results related to the B3LYP/BS2//B3LYP/BS1 calculations are included in the Supporting Information. The atomic orbital populations were calculated on the basis of natural bond orbital (NBO) analyses.[15]

To assess the validity of the BS2 basis set, we repeated the single-point calculations at the M06 level for some selective transition structures using the def2-TZVP (BS3) and def2-QZVP (BS4) basis sets for all elements. The results show that basis set dependence is small. Using the BS2 basis set, the relative energies of $\mathbf{TS}_{2-8}$, $\mathbf{TS}_{2-9}$, $\mathbf{TS}_{4-10}$, $\mathbf{TS}_{11-12}$, $\mathbf{TS}_{12-13}$, $\mathbf{TS}_{11-15}$, and $\mathbf{TS}_{15-13}$ are 29.7, 28.2, 46.6, 24.2, 18.5, 23.5, and 32.2 kcal/mol, respectively. Using the BS3 basis set, the relative energies are 31.2, 29.6, 46.5, 25.8, 20.1, 24.9, 33.7 kcal/mol, respectively. Using the BS4 basis set, the relative energies are 32.3, 30.5 46.7, 26.7, 21.5, 25.8, 34.9 kcal/mol, respectively.

Scheme 3. Relative Stabilities of Various AuCl Adducts

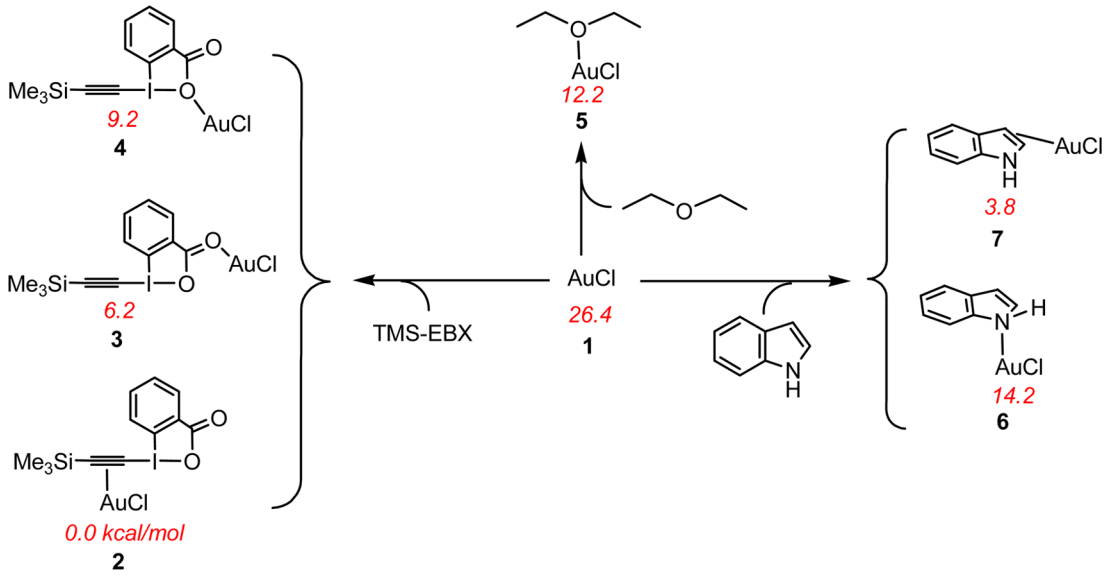

dx.doi.org/10.1021/cs500613t | ACS Catal. 2014, 4, 2896−2907

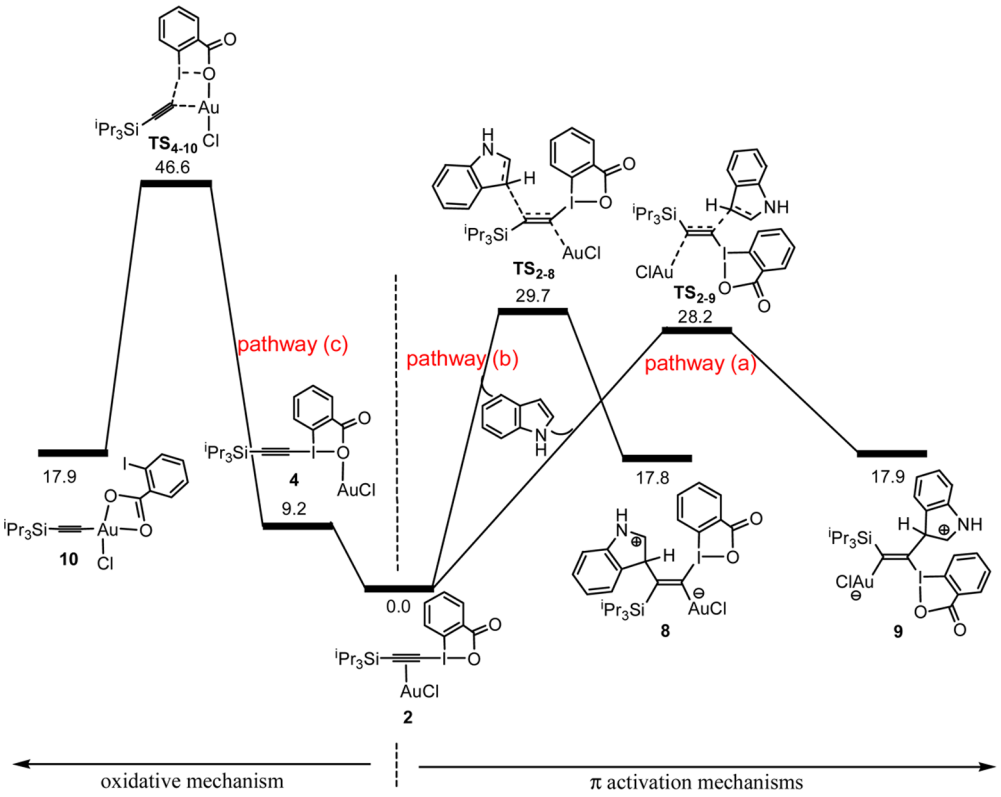

Figure 1. Energy profile calculated for the first step of the three mechanisms shown in Scheme 2 for the indole substrate. The relative Gibbs free energies obtained from the M06/BS2//B3LYP/BS1 calculations in Et_2O are given in units of kcal/mol.

To examine how sensitive our results are to the methodology used for geometry optimizations, the structures of some selective transition states were reoptimized at the M06/BS1 level and then their relative energies were re-evaluated with single-point calculations using the M06/BS3 and M06/BS4 calculations. The results show that there is a small dependence of the relative Gibbs energies on the employed methodology. Using the M06/BS3//M06/BS1 calculations, the relative energies of $\mathbf{TS_{2-8}}$, $\mathbf{TS_{2-9}}$, $\mathbf{TS_{4-10}}$, $\mathbf{TS_{11-12}}$, $\mathbf{TS_{12-13}}$, $\mathbf{TS_{11-15}}$, and $\mathbf{TS_{15-13}}$ are 28.5, 28.1, 45.0, 22.8, 20.0, 22.6, and 33.7 kcal/mol, respectively. Using the M06/BS4//M06/BS1 calculations, the relative energies are 29.6, 29.1, 45.4, 23.8, 21.5, 23.5, 35.1 kcal/mol, respectively.

Since the TIPS substituent in each stationary point has different conformations with different energies, we replaced the TIPS component of TIPS-EBX with trimethylsilane (TMS) to avoid this difficulty. Although we are aware that the less bulky TMS substituent has been experimentally shown to decrease the yield of the organic product,[3b] this replacement is expected not to change the chemistry of the alkynylation reaction.

RESULTS AND DISCUSSION

It is anticipated that the addition of AuCl to substrates and solvent can initially lead to the formation of various adducts, as shown with a few representative examples in Scheme 3. Since, in terms of the Gibbs free energies, **2** is calculated to be the most stable adduct, we consider this structure as the reference point for the gold precursor. As discussed above, three potential mechanisms for the alkynylation of aromatic C−H bonds have been envisaged in the literature (Scheme 2). Figure 1 shows the energy profile calculated for the first step of these three mechanisms for the indole substrate. An inspection of Figure 1 shows that pathways (a) and (b) (Scheme 2) with Gibbs energy barriers of 28.2 and 29.7 kcal/mol, respectively, are energetically more favorable than pathway (c). However, this study allowed us to propose a novel mechanism for the alkynylation reaction. The rate-determining transition structure for this novel mechanism is calculated to lie below $\mathbf{TS_{2-8}}$ and $\mathbf{TS_{2-9}}$ (vide infra), suggesting that the novel mechanism is energetically favored over all the previously proposed mechanisms. The mechanistic details for this new pathway are discussed below.

A Novel Mechanism for Catalytic C−H Alkynylation. Intriguingly, we found that the iodine(III) center is capable of operating as a strong Lewis acid and activating the alkyne moiety more efficiently than AuCl. In order for the π-bond activation by iodine(III) to take place, the transfer of the alkynyl group from I^{III} to Au^{I} should occur first (Figure 2). Starting from **2**, the alkynyl transfer step proceeds through transition structure $\mathbf{TS_{2-11}}$ with an energy barrier of 13.5 to give **11**,[16] in which the iodine(III) center coordinates to the alkyne π-bond. This reaction is calculated to be endergonic by 4.8 kcal/mol, suggesting that the characterization of this intermediate (**11**) should be difficult experimentally, because of its unstable nature. The optimized structures for this key step are shown in Figure 3. The energy required for dissociation of the alkyne moiety in **11** (ΔG = 46.3 kcal/mol) is much greater than that in **2** (ΔG = 26.4 kcal/mol), which indicates that the alkyne binds to iodine(III) more strongly than gold(I). The C^a-C^b bond distance in **11** is calculated to be 0.012 Å longer than that in **2** (Figure 3). It follows from these results that the iodine(III) is a stronger Lewis acid than the Au(I), as evidenced by the lower lying LUMO of **11a** (Scheme 4).

We also found that the alkyne coordinates to the iodine(III) center in **11** asymmetrically; the C^b-I distance is calculated to be 0.345 Å longer than the C^a-I distance (Figure 3). The

dx.doi.org/10.1021/cs500613t | ACS Catal. 2014, 4, 2896−2907

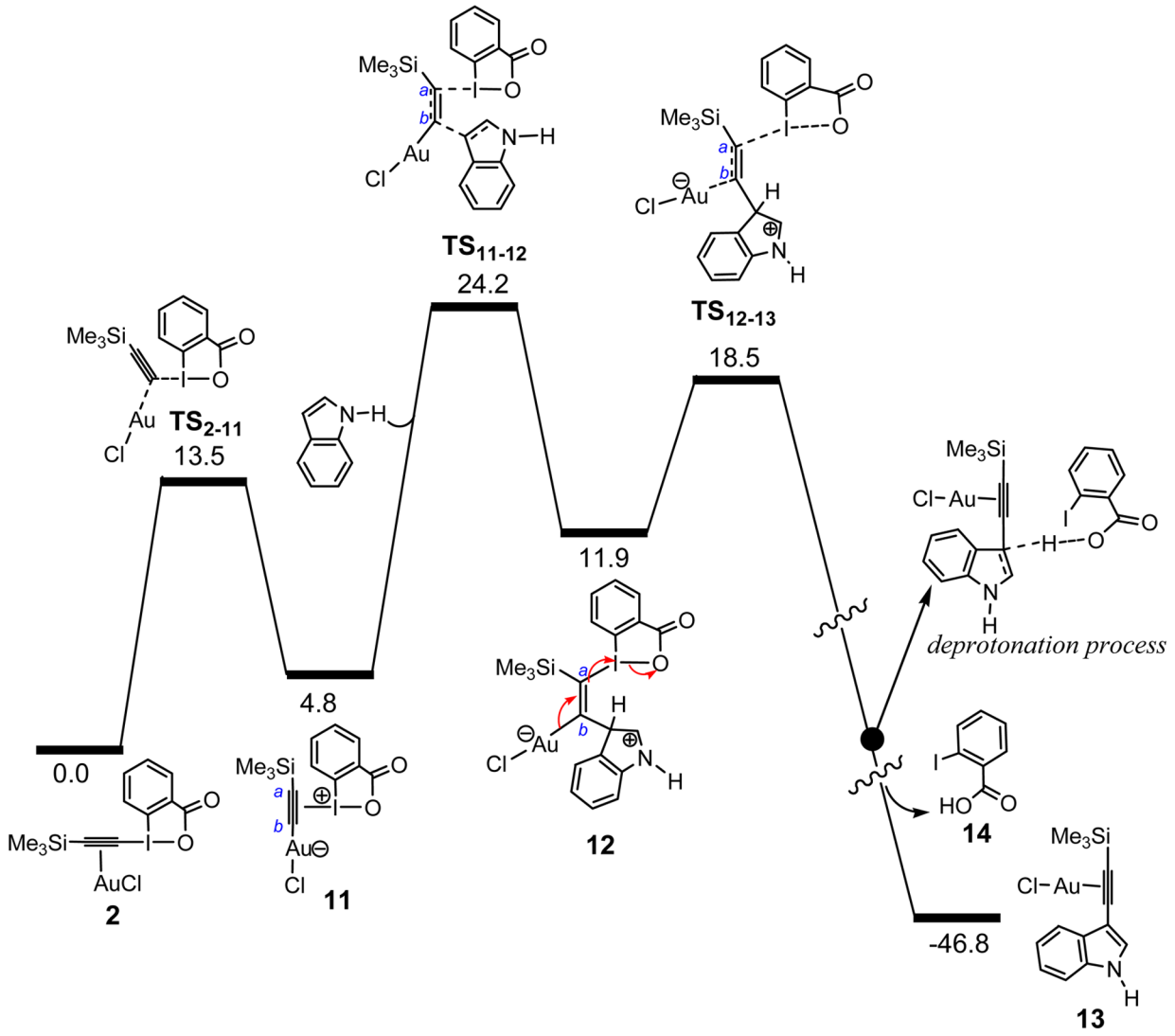

Figure 2. Energy profile calculated for AuCl-catalyzed alkynylation of the indole substrate using TMS-EBX through the novel mechanism. The relative Gibbs free energies obtained from the M06/BS2//B3LYP/BS1 calculations in Et_2O are given in units of kcal/mol.

asymmetric coordination can be related to the π-donating property of AuCl (vide infra), which causes the alkyne π-bond to be polarized toward the C^a atom. In such a case, the C^b atom becomes more electron-deficient and more susceptible to nucleophilic attack. This argument finds support from the NBO analysis of **11**; the population of the C^b p(π)-orbital (0.667 e) is much smaller than that of the C^a p(π)-orbital (1.077 e). At this point, the activated triple bond can undergo the nucleophilic attack of the indole at the C^b atom to give the gold vinyl intermediate **12** through transition structure $\mathbf{TS_{11-12}}$ with an overall activation Gibbs energy of 24.2 kcal/mol[17] (Figure 2). It is striking that this transition structure ($\mathbf{TS_{11-12}}$) is lower in energy than $\mathbf{TS_{2-8}}$ and $\mathbf{TS_{2-9}}$ (Figure 1), indicating that the activation of the alkyne by the iodine(III) center facilitates the nucleophilic attack of the indole. Indeed, the less-stable π-complex **11** is more reactive than the more-stable π-complex **2**. The nucleophilic attack results in one of the π bonds of the alkyne moiety being polarized toward the C^a atom to form the new I−C^a σ-bond in **12**. Upon the indole addition, the I−C^b distance is lengthened from 2.728 Å to 3.122 Å and the I−C^a distance is shortened from 2.383 Å to 2.234 Å (Figure 3).

Starting from the gold vinyl intermediate **12**, there are two possibilities in order for the reaction to proceed toward the formation of product **13**: (a) deprotonation of **12**, using the solvent, followed by the reduction of the iodine(III) and the formation of product **13**; (b) the reduction of the iodine(III) and then the deprotonation reaction. The former is found to be energetically less favorable than the latter. The relative energy of the transition structure for deprotonation of **12** by Et_2O is calculated to be 27.4 kcal/mol (see Figure S1 in the Supporting Information). This pathway is at least 8.9 kcal/mol[18] less favorable than the pathway in which the reduction of iodine(III) occurs first. Thus, we will discuss below only the details related to the pathway that starts with the reduction of iodine(III).

Intriguingly, the reduction of iodine(III) proceeds via transition structure $\mathbf{TS_{12-13}}$ with a Gibbs activation energy as low as 6.6 kcal/mol. The activation energy for this step is also calculated at the B3LYP/BS2//B3LYP/BS2 level to be 0.8 kcal/mol (see Figure S3 in the Supporting Information). These results suggest that the reduction process, in this case, should be extremely fast. In this process, the occupied σ_{Au-C}-orbital interacts with the vacant σ^*_{I-C}-orbital, leading to the heterolytic cleavage of the I−O bond with concomitant formation of a new

dx.doi.org/10.1021/cs500613t | ACS Catal. 2014, 4, 2896−2907

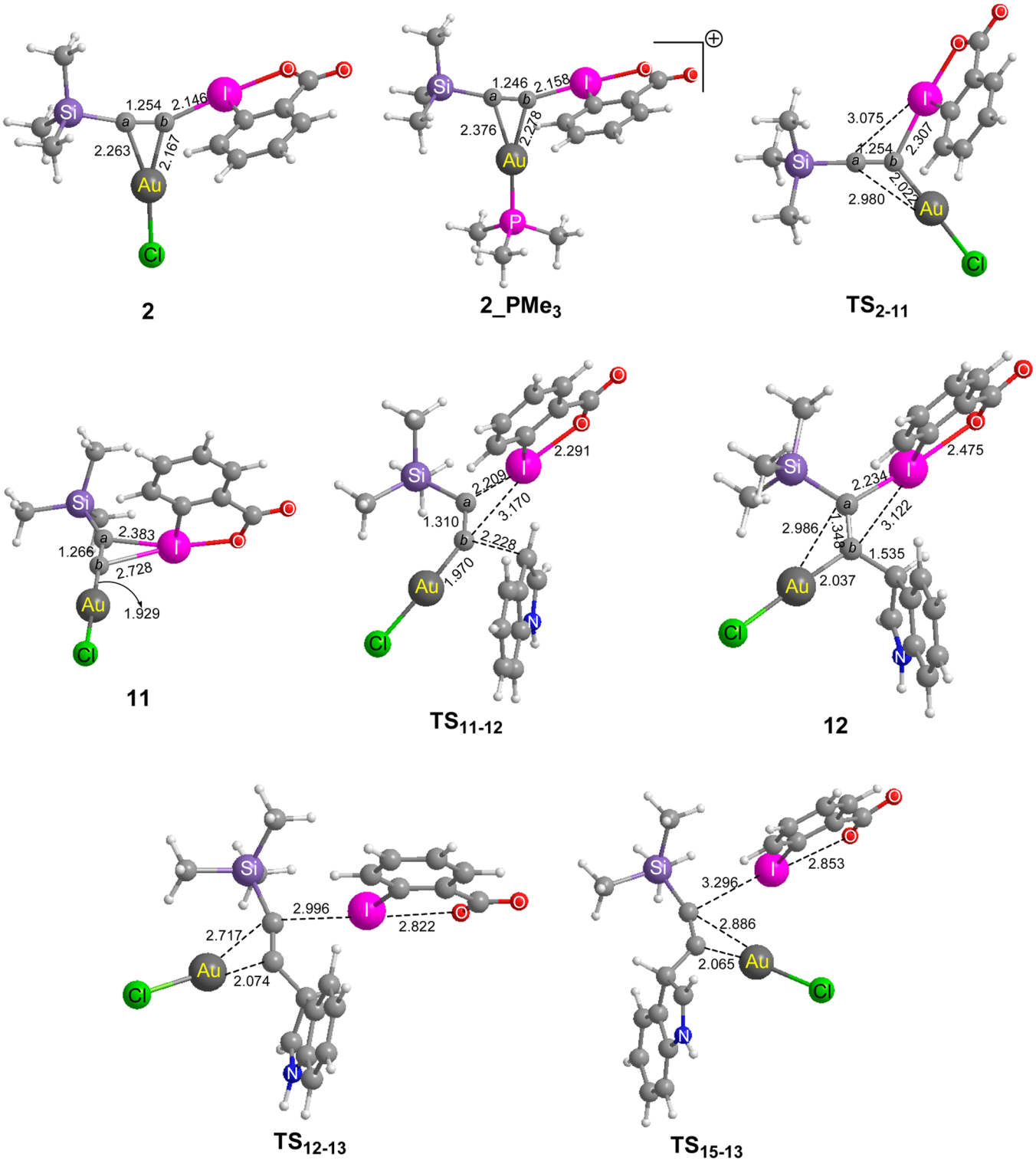

Figure 3. Optimized structures with selected structural parameters (bond lengths given in Ångstroms) for **2**, **2_PMe$_3$**, **TS$_{2-11}$**, **11**, **TS$_{11-12}$**, **12**, **TS$_{12-13}$**, and **TS$_{15-13}$**.

π-bond between the C^a and C^b atoms. This interaction forces the I−C^a σ-bond to be completely polarized toward the I atom, thereby resulting in formation of the 2-iodobenzoate ion through reduction of the iodine by two units. It is interesting to note that the redox process in this case occurs without protonation of the benzoate group, which is usually a prerequisite for reduction of the hypervalent iodine reagents of the type employed here.[19] This finding implies that the presence of the Au−C^b σ-bond at the β-position renders the vinyl group bound to the iodine(III) center in **12** a very strong reducing agent.

An IRC search for **TS$_{12-13}$** shows that this transition structure is directly connected to the product **13**. This result indicates that both the reduction and the deprotonation proceed via a one-step process. Indeed, once the 2-iodobenzoate ion is formed, its strong basicity does not allow this species to remains as a free ion.

dx.doi.org/10.1021/cs500613t | ACS Catal. 2014, 4, 2896−2907

Scheme 4. Spatial Plots of the Lowest Unoccupied Molecular Orbital (LUMO) for 11a and AuCl

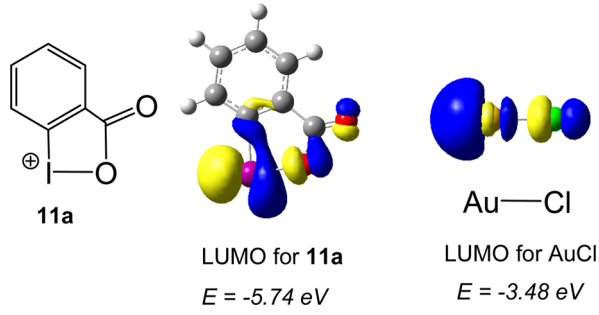

In such a case, the 2-iodobenzoate ion barrierlessly deprotonates the cationic pyrrole group (Figure 2) to give **13** and **14**.

Stereoselectivity of the Arene Addition. There are two pathways for the attack of nucleophiles at activated unsaturated bonds: (*syn* fashion) nucleophilic attack from the side of Lewis acid and (*anti* fashion) nucleophilic attack from the side opposite the Lewis acid. All the above-mentioned results (Figure 2) are concerned with the mechanism in which the indole substrate is added to the activated alkyne via the *syn* fashion. We demonstrate herein that the *anti* addition mechanism is energetically unfavorable. Figure 4 shows the energy profile for formation of **13** through the *anti* addition mechanism. A comparison of the energy profiles given in Figures 2 and 4 reveals that, although the indole addition to the activated alkyne via the *anti* fashion is ~0.7 kcal/mol more favorable than that via the *syn* fashion, the step concerning the reduction of iodine(III) for this pathway is considerably unfavorable; transition structure $\mathbf{TS}_{15-13}$ (Figure 4) lies 13.7 kcal/mol above transition structure $\mathbf{TS}_{12-13}$ (Figure 2). The I−C^a bond distance in $\mathbf{TS}_{15-13}$ is calculated to be 0.3 Å longer than that in $\mathbf{TS}_{12-13}$ (Figure 3), which suggests a later transition state for $\mathbf{TS}_{15-13}$. The difference between these two pathways can be explained by how available the nascent π-bond is for interaction with the Au^I metal center in the transition structures. In transition structure $\mathbf{TS}_{12-13}$, the Au^I metal center easily interacts with the nascent π-bond (Scheme 5a), facilitating the step concerning the reduction of iodine(III) through increasing the stability of the transition structure. In contrast, the nascent π-bond in transition structure $\mathbf{TS}_{15-13}$ is almost blocked by the I atom and, thus, it is not readily available (see Scheme 5b). In such a case, the structure must undergo a significant distortion by lengthening the I−C^a bond in order to make the nascent π-bond more available. The greater the structural distortion, the later the transition state and the higher the activation barrier. On the basis of these results, we conclude that the Au^I-catalyzed alkynylation reactions should occur through the *syn* addition pathway in diethyl ether.

Proposed Catalytic Cycle for C−H Alkynylation. The detailed catalytic cycle of the Au^I-catalyzed alkynylation reaction using a hypervalent iodine(III) reagent is summarized in Scheme 6. This unprecedented mechanism includes five major steps: (A)

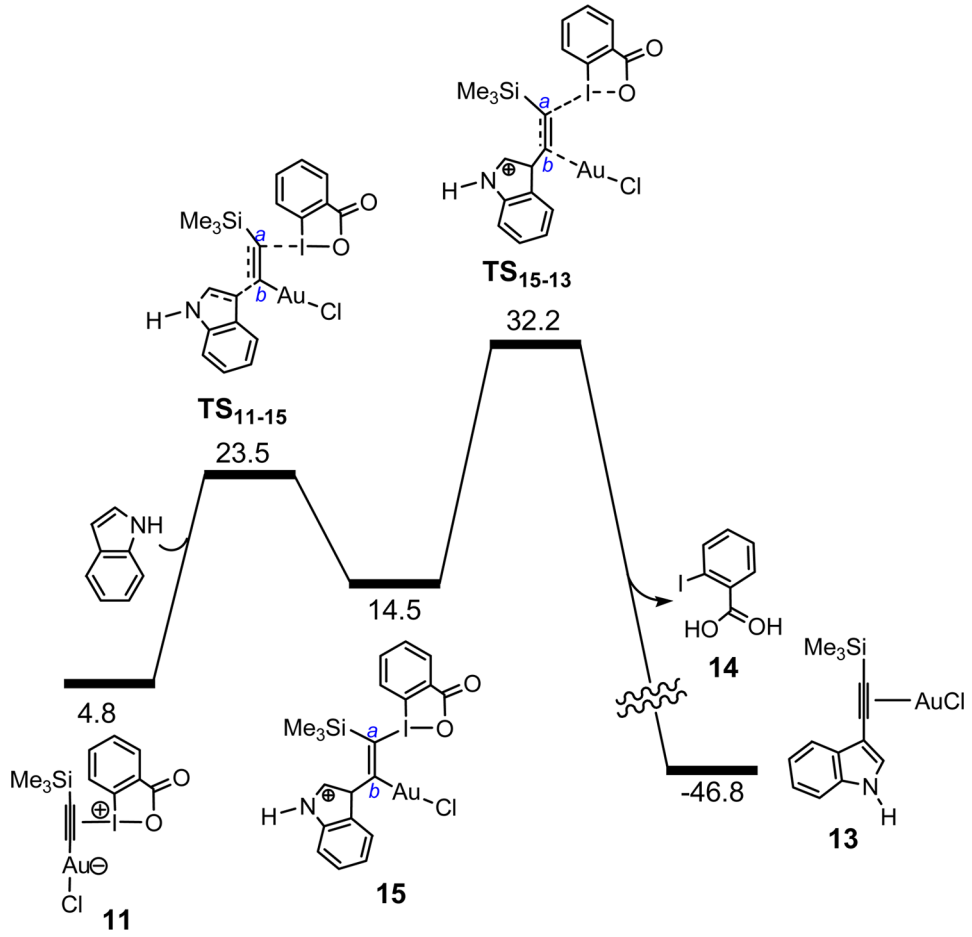

Figure 4. Energy profile calculated for the catalytic C−H alkynylation initiated by *anti* addition of the indole substrate. The relative Gibbs free energies obtained from the M06/BS2//B3LYP/BS1 calculations in Et_2O are given in units of kcal/mol.

dx.doi.org/10.1021/cs500613t | ACS Catal. 2014, 4, 2896−2907

Scheme 5. Schematic Orbital Interactions Rationalizing the Higher Stability of TS_{12-13} Relative to TS_{15-13}

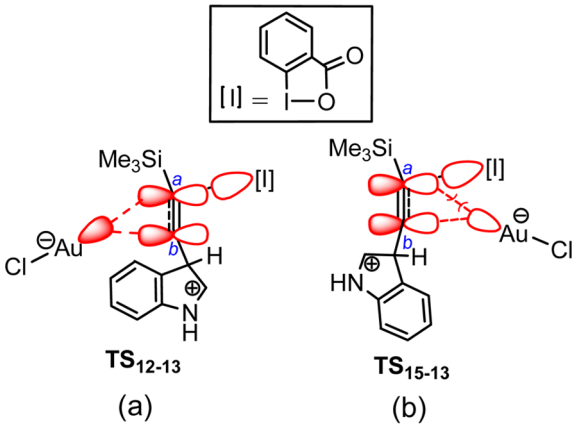

coordination of the alkyne moiety of the iodine(III) reagent to the AuCl catalyst, (B) transfer of the alkynyl group from I^{III} to Au^{I}, (C) a Friedel–Crafts-type addition of the arene to the C^b atom of the iodine(III)-activated alkyne via the *syn* fashion, (D) reduction of the iodine(III) by two units through interaction of the Au–C^b σ-orbital with the I–C^a σ^*-orbital, and (E) deprotonation of the cationic pyrrole group by the 2-iodobenzoate ion. The calculations predict that step C is the rate-determining step[20] and step E occurs immediately, once the reduction step is complete. To our knowledge, this is the first investigation which suggests that an unsaturated triple bond is activated by iodine(III) toward nucleophiles.

The recent experimental reports further support the validity of our results. Waser and co-workers demonstrated that the alkynylation of less-nucleophilic arenes such as thiophenes and benzofurans is feasible if the gold-catalyzed reaction is carried out in the presence of an acid as a co-activator.[2b,g,3b] On the other hand, it is well-established that Lewis or Brønsted acids are capable of enhancing the electrophilicity and reactivity of hypervalent iodine reagents.[19] These experimental observations agree well with the outcome of the calculations that the rate-determining step for the alkynylation is the arene addition to the iodine(III)-activated alkyne. It is expected that the acids increase the electrophilicity of the iodine(III) center, thereby accelerating the addition of the less-nucleophilic arenes to the iodine(III)-activated alkyne. The confirmation of this statement is the objective of an ongoing project.

The calculations at the B3LYP/BS2//B3LYP/BS1 level further support the results obtained from the M06/BS2//B3LYP/BS1 functional (see Figures S2–S4 in the Supporting Information) and confirm that the mechanism given in Scheme 6 is energetically more favorable than other previously proposed mechanisms.

Origin of Regioselectivity for the Catalytic C–H Alkynylation of Arenes. As stated in the Introduction, the regioselectivity of the catalytic C–H alkynylation is reliant on the identity of the aromatic substrates. Waser and co-workers demonstrated that the alkynylation for indoles occurs at C3 and for pyrroles at C2. The product selectivity was explained in terms of the electron richness of the C2 and C3 centers.[4d] Here, we will show that the thermodynamic stability of the intermediates obtained from the Friedel–Crafts addition of the arenes onto intermediate **11** can be utilized as a predictor for the regioselectivity.

As already mentioned, the rate-determining step of the C–H alkynylation is step C (Scheme 6). Therefore, one expects that

Scheme 6. A Novel Mechanism for the Alkynylation of the Indole Substrate

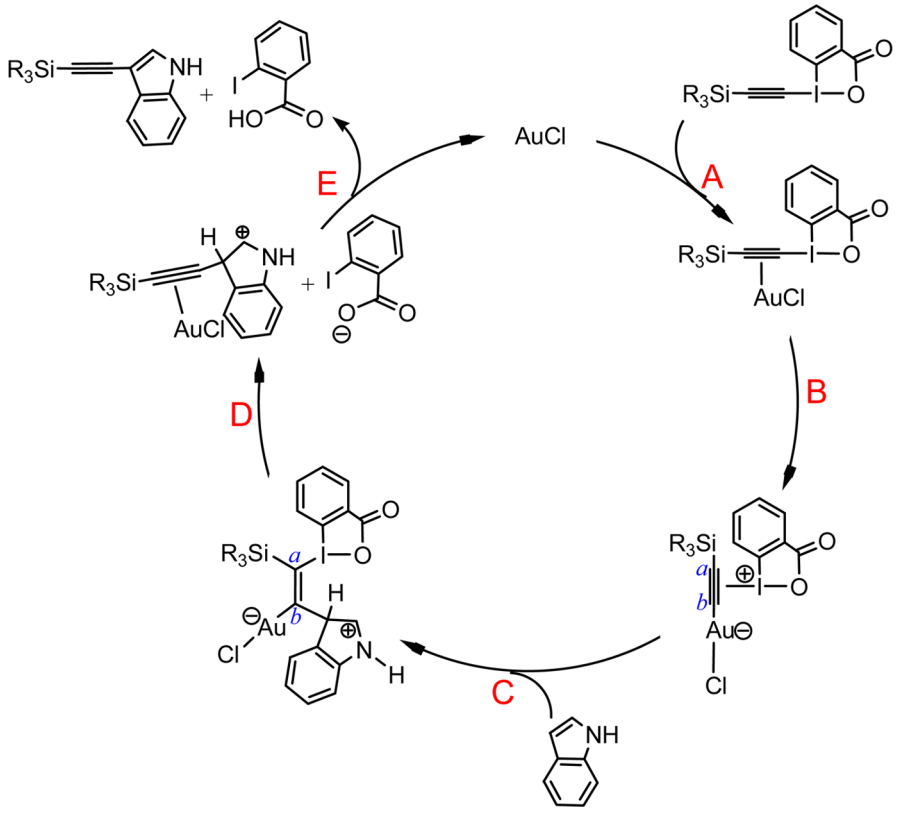

dx.doi.org/10.1021/cs500613t | ACS Catal. 2014, 4, 2896–2907

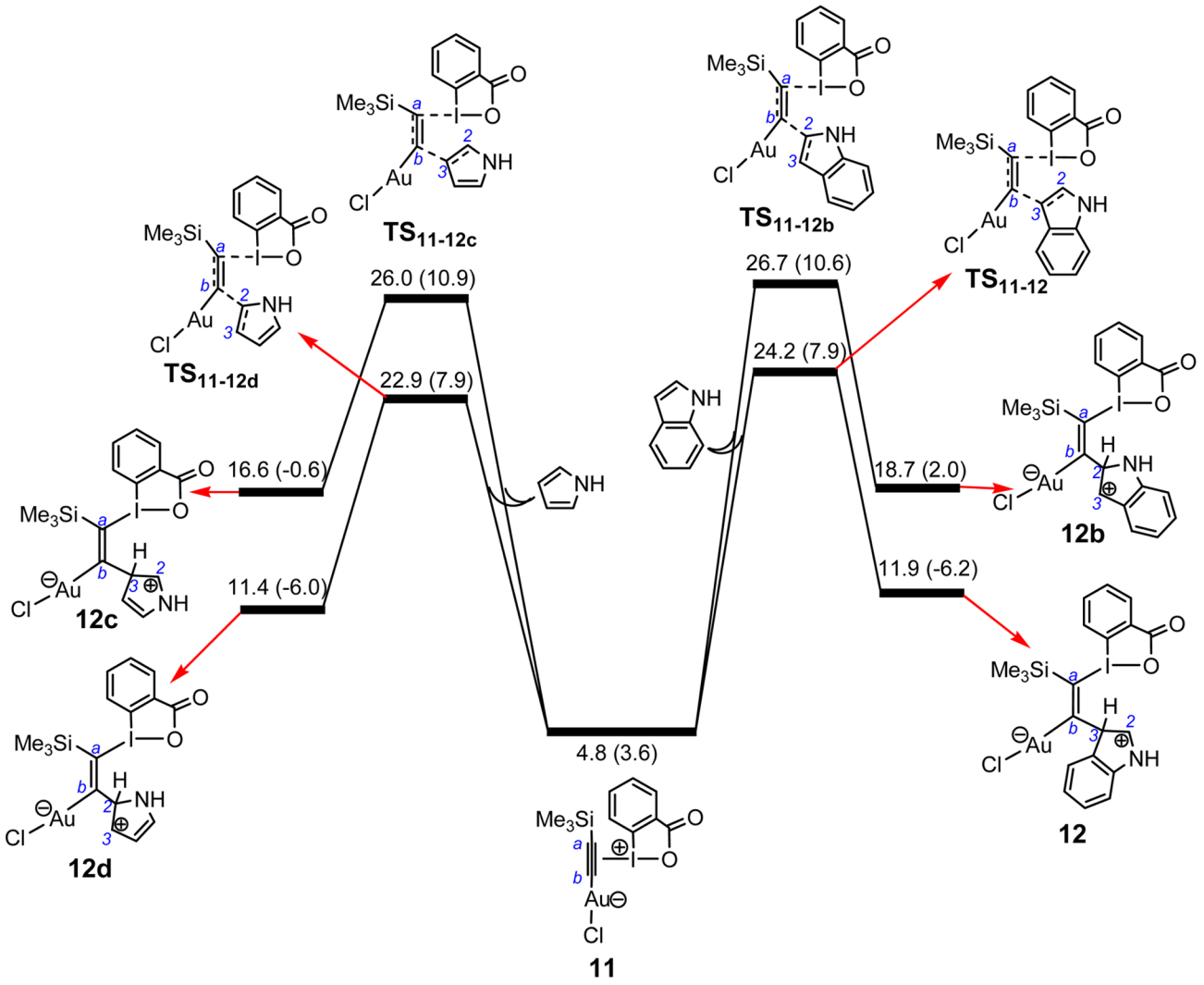

Figure 5. An energy profile comparing the nucleophilic attack of the indole and pyrrole substrates to the iodine(III)-activated alkyne via the C2 and C3 atoms. The relative Gibbs and electronic energies (in parentheses) obtained from the M06/BS2//B3LYP/BS1 calculations in Et_2O are given in units of kcal/mol.

the regioselectivity is dictated by the barrier height of this step. For the indole substrate, $\mathbf{TS}_{11-12}$ is calculated to be 2.5 kcal/mol lower in energy than $\mathbf{TS}_{11-12b}$ (Figure 5), indicating that, in agreement with the experiment, the alkynylation at the C3 atom is energetically favored over that at the C2 atom. In contrast, for the pyrrole substrate, $\mathbf{TS}_{11-12d}$ lies 3.1 kcal/mol below $\mathbf{TS}_{11-12c}$ (Figure 4), implying that the alkynylation reaction preferentially occurs at the C2 atom of the pyrrole. An inspection of the results (Figure 5) shows that there exists a relationship between energies of the transition structures and the gold vinyl intermediates: the more stable the gold vinyl intermediate, the lower the activation energy. We found an excellent correlation with an R^2 value of 0.99 for the plot of ΔE against $\Delta E^{\ddagger}$ values (Figure 6). This correlation suggests that, regardless of the identity of the heteroarene, the ease of the C−H alkynylation reaction is directly affected by the thermodynamic stability of the gold vinyl intermediate. The rationale behind the stability of the vinyl intermediates is given in the Supporting Information.

Origin of Unreactivity of Cationic Gold Complexes for the Alkynylation Reaction. Waser and co-workers demonstrated that the cationic gold complexes such as PPh_3Au^+ are not active toward alkynylation. To understand why this is the case,

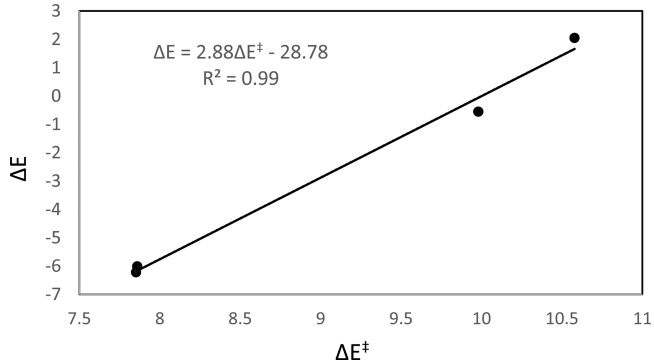

Figure 6. Plot of the values of ΔE against $\Delta E^{\ddagger}$ for the addition of the indole and pyrrole substrates to the iodine(III)-activated alkyne via the C2 and C3 atoms (see Figure 5).

calculations were carried out to probe the alkynylation reaction using PMe_3Au^+ as a model catalyst (Figure 7). The overall barrier for the PMe_3Au^+-catalyzed alkynylation (23.2 kcal/mol) is comparable to that for the AuCl-catalyzed alkynylation (24.2 kcal/mol; see Figure 2). This result suggests that the nature of the gold(I) catalyst does not affect the overall activation barrier if

dx.doi.org/10.1021/cs500613t | ACS Catal. 2014, 4, 2896−2907

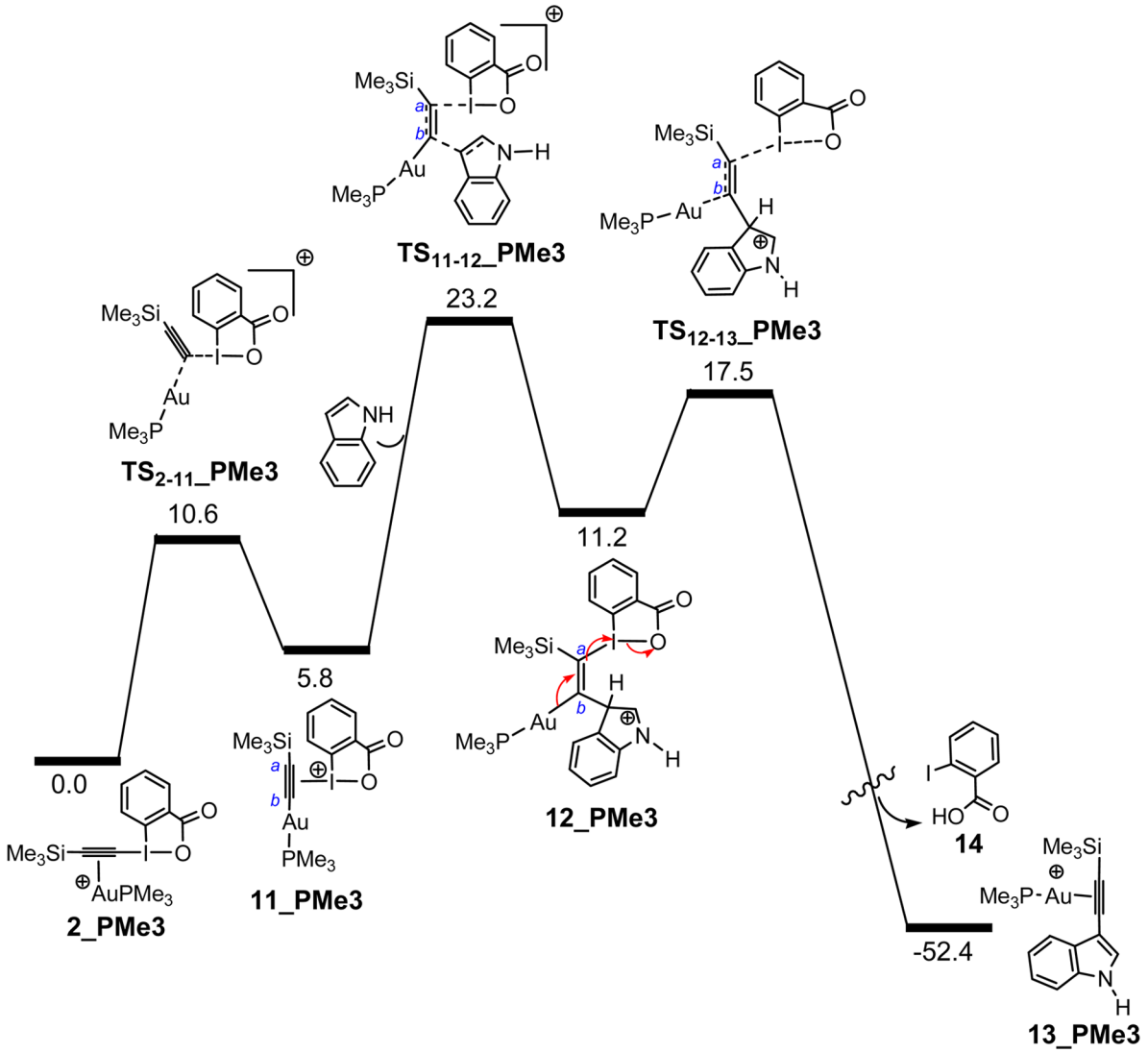

Figure 7. Energy profile calculated for PMe_3Au^+-catalyzed alkynylation of the indole substrate using TMS-EBX through the novel mechanism. The relative Gibbs free energies obtained from the M06/BS2//B3LYP/BS1 calculations in Et_2O are given in units of kcal/mol.

the alkyne π-complexes (**2** or **2_PMe3**) are considered as the reference point. Initially, this result appears to conflict with the experimental data. However, we found that the difference in reactivity is mainly due to a change in the nature of the catalyst resting state. As mentioned previously (Scheme 3), the alkyne π-complex **2** is the resting state for the AuCl system from which the alkynylation reaction is initiated. In contrast, the resting state for the PMe_3Au^+ system changes from the active π-complex to the inactive O-bound complex **3_PMe3** (Scheme 7); the O-bound complex has lower energy by 5.7 kcal/mol. In such a case, the cationic catalysts are expected to be "poisoned" by coordination to the carbonyl group of the benzoate moiety to initially give the inactive O-bound complex **3_PMe3**. Under these circumstances, the real activation barrier for the alkynylation reaction using PMe_3Au^+ as the catalyst is calculated to be as high as 28.9 kcal/mol and not 23.3 kcal/mol (Scheme 7).

This discrepancy between AuCl and PMe_3Au^+ is attributed to the stronger coordination of the alkyne triple bond to AuCl (~9.8 kcal/mol), which is due to the more electron-rich character of the metal center of AuCl. In such a case, a stronger gold-to-alkyne back-donation is predicted for the AuCl system. To support this statement, the charge decomposition analysis for adducts **2** and **2_PMe3** was performed using the CDA method.[21] The result of the CDA calculation indicates that the back-donation from gold to the alkyne in **2** is significant ($b/d = 0.251$) while that in **2_PMe3** is negligible ($b/d = 0.085$).[22] The presence of the positive charge in the PMe_3Au^+ system is expected to be responsible for disfavoring the back-donation interaction. A comparison of the structural parameters of **2_PMe3** and **2** (Figure 3) shows that the less-favorable back-donation in **2_PMe3** results in longer Au−C^a and Au−C^b distances and shorter C^a−C^b distances.

By analogy with the M06 functional, **2_PMe3** is calculated at the B3LYP/BS2//B3LYP/BS1 level to be 9.8 kcal/mol less stable than **3_PMe3**. Taking this result into account, the overall activation barrier for the alkynylation at the B3LYP/BS2//B3LYP/BS1 level increases to 43.1 kcal/mol (see Figure S5 in the Supporting Information). Thus, the present calculations show that the cationic gold systems are not active for the alkynylation reaction, because they strongly prefer to coordinate to the benzoate groups to form the inactive O-bound adducts.

Can a Gold(III) or Gold(0) Species Act as an Active Catalyst? AuCl is sometimes degraded in solution to give $AuCl_3$ and Au^0.[23] If we assume that this degradation occurs during the

dx.doi.org/10.1021/cs500613t | ACS Catal. 2014, 4, 2896−2907

Scheme 7. Relative Stabilities of Various PMe_3Au^+ Adducts and Transition Structure TS_{11-12_PMe3}

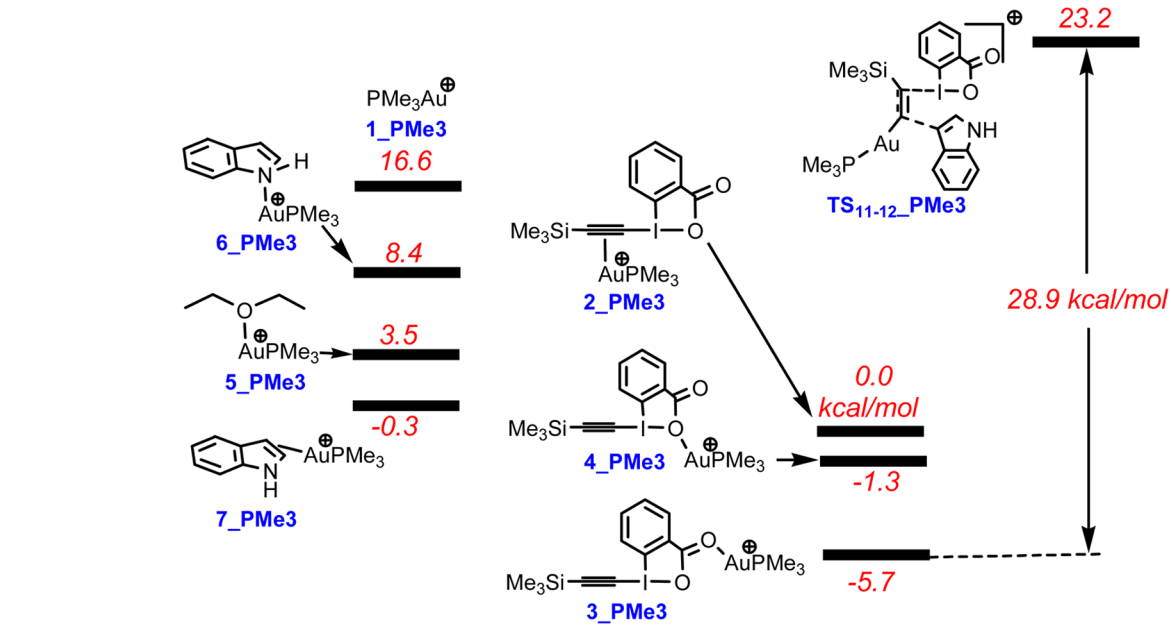

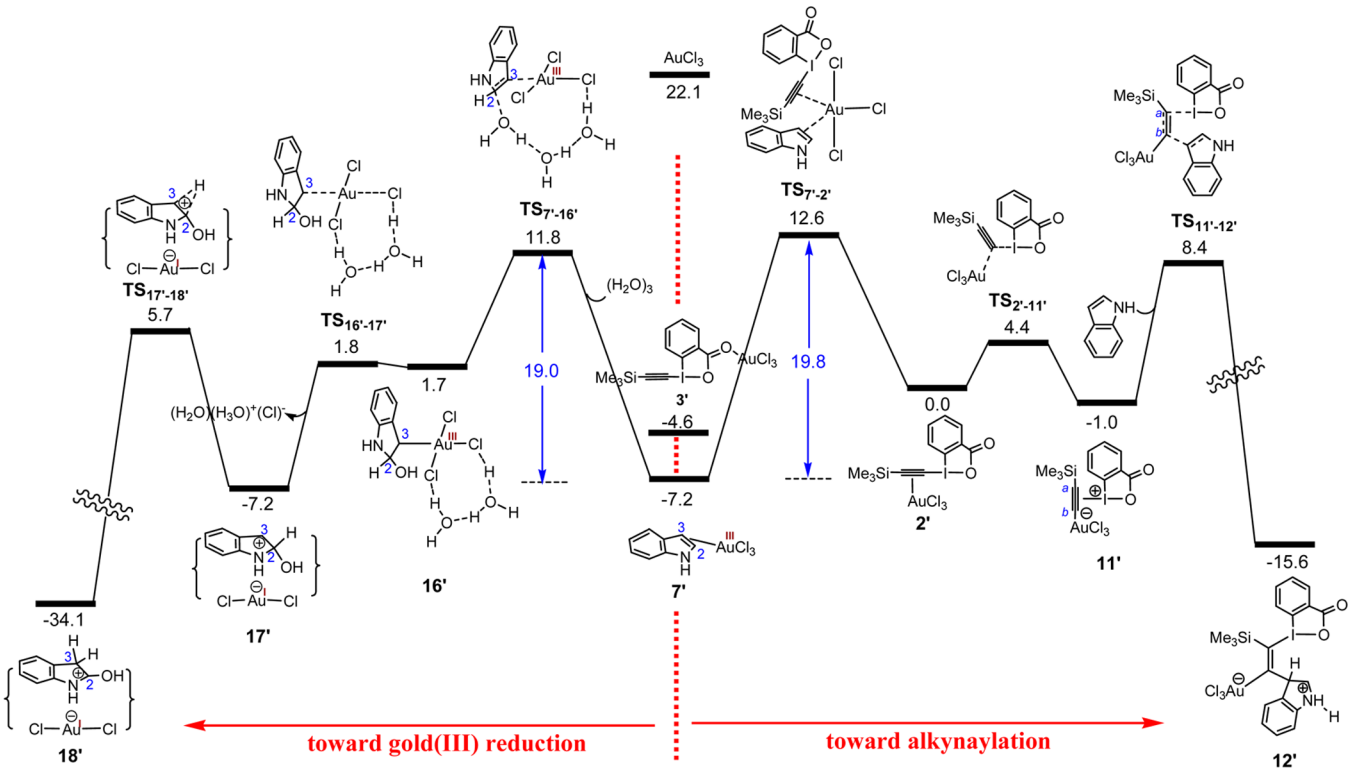

Figure 8. Energy profile comparing the $AuCl_3$-catalyzed alkynylation of the indole substrate with a pathway leading to the reduction of gold(III). The relative Gibbs free energies obtained from the M06/BS2//B3LYP/BS1 calculations in Et_2O are given in units of kcal/mol.

course of the alkynylation reaction, one may inquire whether or not the catalytic activity can be attributed to the in situ formation of $AuCl_3$ or Au^0. To address this issue, the catalytic cycle given in Scheme 6 was reinvestigated by replacing AuCl with $AuCl_3$ or a gold(0) nanoparticle. According to the study carried out by Robinson et al.,[24] a three-membered cluster (Au_3Cl) was chosen as an model for the gold(0) nanoparticle.

The resting state in the $AuCl_3$ catalytic cycle is calculated to be **7′** (see Figure 8). Thus, in order for the active π-complex **2′** to be formed, **7′** should undergo an associative substitution by the alkyne substrate via the five-coordinate transition structure $TS_{7'-2'}$. The activation Gibbs energy for this process is computed to be 19.8 kcal/mol. The key intermediate **11′** is then formed via transition structure $TS_{2'-11'}$. The calculations show that **11′** is much more reactive than its Au^I analogue (**11** in Figure 2); the energy barrier for conversion of **11′** + indole → **12′** (9.1 kcal/mol) is far smaller than that for conversion of **11** + indole → **12** (19.4 kcal/mol). The high reactivity of **11′** can be ascribed to the

dx.doi.org/10.1021/cs500613t | ACS Catal. 2014, 4, 2896−2907

lack of electron back-donating capability of the gold(III) center and the strong Au−C bond in **12′**, as evidenced by an exergonicity of −14.6 for the transformation of **11′** to **12′**.

These results suggest that the Au^{III}-catalyzed alkynylation reaction should be facile, provided that the substitution reaction occurs first. However, there are other competitive pathways starting from **7′**, leading to the reduction of gold(III), thereby inhibiting the catalytic activity of this catalyst. For example, water molecules are found to be capable of reducing the gold(III) center via their nucleophilic attack to the C2 atom of indole in **7′** (Figure 8) (the C2 atom is more electron-deficient than the C3 atom). The nucleophilic attack increases the electron density on the C3 atom and turns the ring in **16′** into a strong reducing agent. The electron transfer from the ring to the Au $d_{x^2-y^2}$-orbital results in heterolytic cleavage of a Au−Cl bond and formation of an ion pair (**17′** in Figure 8) in which the gold(I) complex $[AuCl_2]^-$ is mainly stabilized by an electrostatic interaction with a carbocation. A 1,2-hydrogen shift process renders the ion pair even more stable and leads to the formation of **18′**. The mechanism presented here for the gold(III) reduction is similar to that reported for Pt(IV) reduction by a guanine.[25]

Nucleophilic attack is calculated to be the rate-determining step for the gold(III) reduction process. The transition structure for this step ($\mathbf{TS}_{7'-16'}$) lies 0.8 kcal/mol lower in energy than $\mathbf{TS}_{7'-2'}$, suggesting that the reduction of gold(III) is slightly more favorable than the substitution reaction. It follows from these calculations that the alkynylation of indoles is less likely to take place on a gold(III) catalyst, because this catalytic reaction is competitive with the gold(III) reduction process. These results are in close agreement with the experimental observations; Waser and co-workers demonstrated that a gold(III) complex is reduced in situ by a indole substrate into a gold(I) species, although the reaction conditions precluded identification of the indole oxidation product. They also confirmed that the gold species derived from the reduction process are reactive toward the alkynylation reaction, further supporting the assumption that the active catalyst for the reaction is most likely a gold(I) species. At the end of this section, it should be mentioned that, since the product of the indole oxidation was not identified experimentally, finding a precise mechanism for the gold(III) reduction process is impossible and this study at least suggests that water nucleophiles have the capability of reducing the gold(III) center in **7′** at a rate comparable to the alkynylation reaction.

The possibility that gold(0) nanoparticles are responsible for catalyzing the reaction was also investigated by using the three-member cluster Au_3Cl as a model catalyst. In this case, the nucleophilic attack of the indole substrate to the I^{III}-activated alkyne has a calculated activation barrier of 29.9 kcal/mol (see Figure S6 in the Supporting Information), implying that the reactivity of Au_3Cl toward the alkynylation reaction is less than that of AuCl. It can be suggested from these results that a gold nanoparticle is less likely to catalyze the alkynylation reaction, although further investigation in this regard is still needed.

CONCLUSION

Density functional theory (DFT) calculations were performed to investigate the mechanism of AuCl-catalyzed alkynylation of the indole and pyrrole substrates using a hypervalent iodine reagent (TMS-EBX). The catalytic reaction starts with coordination of the alkyne moiety of the iodine(III) reagent to the AuCl catalyst, followed by transfer of the alkynyl group from I^{III} to Au^{I}. Because of the stronger acidic character of the iodine(III) center, the alkyne triple bond is activated more effectively by coordination to the iodine(III) center. The nucleophilic attack of the aromatic substrates to the I^{III}-activated alkyne is predicted to be the rate-determining step and leads to the formation of a iodine(III) gold(I) vinyl complex. The presence of the Au−C bond at the β-position of the iodine(III) center in the vinyl complex converts the vinyl group to a very strong reducing agent. The reducing character increases when the Au−C bond adopts an *anti* configuration, relative to the I−C bond. In such a case, the iodine(III) is easily reduced by two units via the interaction of the occupied σ_{Au-C}-orbital with the vacant σ^*_{I-C}-orbital and finally the 2-iodobenzoate ion is formed. It is interesting to note that, due to the reducing character of the vinyl group, the vinyl complex does not need to undergo protonation at the benzoate group prior to reduction process. In the last step, a very fast deprotonation process by the 2-iodobenzoate ion gives the alkynylation product.

The regioselectivity of nucleophilic attack of arenes is controlled by the stability of the vinyl complexes. The cationic gold complexes such as PMe_3Au^+ are not effective catalysts for the alkynylation reaction because they are strongly poisoned by coordination to the benzoate group of the iodine(III) reagent. The insight provided by the present theoretical study helps expand the scope of benziodoxolone-based alkynylation reactions to design new catalysts for similar reactions.

ASSOCIATED CONTENT

Supporting Information

Text giving the complete ref 5; a table giving Cartesian coordinates of all optimized structures along with energies; figures giving the energy profiles calculated at the B3LYP/BS2//B3LYP/BS1 level; energy profiles for deprotonation of **12**; an energy profile for Au_3Cl-catalyzed alkynylation of indole; and a discussion about the rationale behind the stability of the vinyl intermediates. This material is available free of charge via the Internet at http://pubs.acs.org.

AUTHOR INFORMATION

Corresponding Author

*E-mail: Alireza.Ariafard@utas.edu.au.

Notes

The authors declare no competing financial interest.

ACKNOWLEDGMENTS

The author thanks the Australian National Computational Infrastructure and the University of Tasmania for computing resources. The author is also grateful for the financial support of the Islamic Azad University, Central Tehran Branch. The author also thanks Prof. Allan Canty for his valuable advice during the completion of this study.

REFERENCES

(1) (a) Seregin, I. V.; Ryabova, V.; Gevorgyan, V. *J. Am. Chem. Soc.* **2007**, *129*, 7742−7743. (b) Tobisu, M.; Ano, Y.; Chatani, N. *Org. Lett.* **2009**, *11*, 3250−3252. (c) Besselievre, F.; Piguel, S. *Angew. Chem., Int. Ed.* **2009**, *48*, 9553−9556. (d) Matsuyama, N.; Hirano, K.; Satoh, T.; Miura, M. *Org. Lett.* **2009**, *11*, 4156−4159. (e) Kim, S. H.; Chang, S. *Org. Lett.* **2010**, *12*, 1868−1871. (f) Wei, Y.; Zhao, H.; Kan, J.; Su, W.; Hong, M. *J. Am. Chem. Soc.* **2010**, *132*, 2522−2523. (g) Matsuyama, N.; Kitahara, M.; Hirano, K.; Satoh, T.; Miura, M. *Org. Lett.* **2010**, *12*, 2358−2361. (h) Lauterbach, T.; Livendahl, M.; Rosellon, A.; Espinet, P.; Echavarren, A. M. *Org. Lett.* **2010**, *12*, 3006−3009. (i) Yao, Bo; Wang, Q.; Zhu, J. *Angew. Chem., Int. Ed.* **2012**, *51*, 12311−12315. (j) Ano, Y.;

Tobisu, M.; Chatani, N. *Org. Lett.* **2012**, *14*, 354−357. (k) Jie, X.; Shang, Y.; Hu, P.; Su, W. *Angew. Chem., Int. Ed.* **2013**, *52*, 3630−3633.
(2) (a) de Haro, T.; Nevado, C. *J. Am. Chem. Soc.* **2010**, *132*, 1512−1513. (b) Brand, J. P.; Waser, J. *Angew. Chem., Int. Ed.* **2010**, *49*, 7304−7307. (c) Lubriks, D.; Sokolovs, I.; Suna, E. *J. Am. Chem. Soc.* **2012**, *134*, 15436−15442. (d) Brand, J. P.; Waser, J. *Org. Lett.* **2012**, *14*, 744−747. (e) Li, Y.; Brand, J. P.; Waser, J. *Angew. Chem., Int. Ed.* **2013**, *52*, 6743−6747. (f) Tolnai, G. L.; Ganss, S.; Brand, J. P.; Waser, J. *Org. Lett.* **2013**, *15*, 112−115. (g) Li, Y.; Waser, J. *Beilstein J. Org. Chem.* **2013**, *9*, 1763−1767. (h) Xie, F.; Qi, Z.; Yu, S.; Li, X. *J. Am. Chem. Soc.* **2014**, *136*, 4780−4787. (i) Nierth, A.; Marletta, M. A. *Angew. Chem., Int. Ed.* **2014**, *53*, 2611−2614. (j) Feng, C.; Loh, T.-P. *Angew. Chem., Int. Ed.* **2014**, *53*, 2722−2726. (k) Collins, K. D.; Lied, F.; Glorius, F. *Chem. Commun.* **2014**, *50*, 4459−4461.
(3) (a) Brand, J. P.; Charpentier, J.; Waser, J. *Angew. Chem., Int. Ed.* **2009**, *48*, 9346−9349. (b) Brand, J. P.; Chevalley, C.; Scopelliti, R.; Waser, J. *Chem.—Eur. J.* **2012**, *18*, 5655−5666.
(4) (a) Garcia, P.; Malacria, M.; Aubert, C.; Gandon, V.; Fensterbank, L. *ChemCatChem* **2010**, *2*, 493−497. (b) Wegner, H. A.; Auzias, M. *Angew. Chem., Int. Ed.* **2011**, *50*, 8236−8247. (c) Brand, J. P.; Waser, J. *Chem. Soc. Rev.* **2012**, *41*, 4165−4179. (d) Brand, J. P.; Li, Y.; Waser, J. *Isr. J. Chem.* **2013**, *53*, 901−910.
(5) Frisch, M. J.; Trucks, G. W.; Schlegel, H. B.; Scuseria, G. E.; Robb, M. A.; Cheeseman, J. R.; Scalmani, G.; Barone, V.; Mennucci, B.; Petersson, G. A.; Nakatsuji, H.; Caricato, M.; Li, X.; Hratchian, H. P.; Izmaylov, A. F.; Bloino, J.; Zheng, G.; Sonnenberg, J. L.; Hada, M.; Ehara, M.; Toyota, K.; Fukuda, R.; Hasegawa, J.; Ishida, M.; Nakajima, T.; Honda, Y.; Kitao, O.; Nakai, H.; Vreven, T.; Montgomery, J. A.; , Jr., Peralta, J. E.; Ogliaro, F.; Bearpark, M.; Heyd, J. J.; Brothers, E.; Kudin, K. N.; Staroverov, V. N.; Kobayashi, R.; Normand, J.; Raghavachari, K.; Rendell, A.; Burant, J. C.; Iyengar, S. S.; Tomasi, J.; Cossi, M.; Rega, N.; Millam, J. M.; Klene, M.; Knox, J. E.; Cross, J. B.; Bakken, V.; Adamo, C.; Jaramillo, J.; Gomperts, R.; Stratmann, R. E.; Yazyev, O.; Austin, A. J.; Cammi, R.; Pomelli, C.; Ochterski, J. W.; Martin, R. L.; Morokuma, K.; Zakrzewski, V. G.; Voth, G. A.; Salvador, P.; Dannenberg, J. J.; Dapprich, S.; Daniels, A. D.; Farkas, O.; Foresman, J. B.; Ortiz, J. V.; Cioslowski, J.; Fox, D. J. *Gaussian 09, Revision A.02*; Gaussian, Inc.: Wallingford, CT, 2009.
(6) (a) Lee, C. T.; Yang, W. T.; Parr, R. G. *Phys. Rev. B* **1988**, *37*, 785−789. (b) Miehlich, B.; Savin, A.; Stoll, H.; Preuss, H. *Chem. Phys. Lett.* **1989**, *157*, 200−206. (c) Becke, A. D. *J. Chem. Phys.* **1993**, *98*, 5648−5652.
(7) Barone, V.; Cossi, M. *J. Phys. Chem. A* **1998**, *102*, 1995−2001.
(8) (a) Hay, P. J.; Wadt, W. R. *J. Chem. Phys.* **1985**, *82*, 270−283. (b) Wadt, W. R.; Hay, P. J. *J. Chem. Phys.* **1985**, *82*, 284−298.
(9) Hariharan, P. C.; Pople, J. A. *Theor. Chim. Acta* **1973**, *28*, 213−222.
(10) (a) Ehlers, A. W.; Böhme, M.; Dapprich, S.; Gobbi, A.; Höllwarth, A.; Jonas, V.; Köhler, K. F.; Stegmann, R.; Veldkamp, A.; Frenking, G. *Chem. Phys. Lett.* **1993**, *208*, 111−114. (b) Höllwarth, A.; Böhme, M.; Dapprich, S.; Ehlers, A. W.; Gobbi, A.; Jonas, V.; Köhler, K. F.; Stegmenn, R.; Veldkamp, A.; Frenking, G. *Chem. Phys. Lett.* **1993**, *208*, 237−240.
(11) (a) Fukui, K. *J. Phys. Chem.* **1970**, *74*, 4161−4163. (b) Fukui, K. *Acc. Chem. Res.* **1981**, *14*, 363−368.
(12) Zhao, Y.; Truhlar, D. G. *Acc. Chem. Res.* **2008**, *41*, 157−167.
(13) Weigend, F.; Furche, F.; Ahlrichs, R. *J. Chem. Phys.* **2003**, *119*, 12753−12762.
(14) Sieffert, N.; Bühl, M. *Inorg. Chem.* **2009**, *48*, 4622−2624.
(15) Glendening, E. D.; Read, A. E.; Carpenter, J. E.; Weinhold, F. *NBO, version 3.1*; Gaussian, Inc.: Pittsburgh, PA, 2003.
(16) The activation barrier for oxidation of gold(I) from **11** is calculated to be 46.8 kcal/mol, further supporting the claim that the oxidative addition mechanism is not favorable.
(17) The real activation Gibbs free energy is expected to be significantly lower than 24.2 kcal/mol because the rotational and translational contributions to the entropy change is overestimated by the calculation. A precise estimate of the entropy change is too difficult to calculate. See: (a) Tamura, H.; Yamasaki, H.; Sato, H.; Sakaki, S. *J. Am. Chem. Soc.* **2003**, *125*, 16114−16126. (b) Sakaki, S.; Takayama, T.; Sumimoto, M.; Sugimoto, M. *J. Am. Chem. Soc.* **2004**, *126*, 3332−3348. (c) Braga, A. C.; Ujaque, G.; Maseras, F. *Organometallics* **2006**, *25*, 3647−3658. (d) Ariafard, A.; Ejehi, Z.; Sadrara, H.; Mehrabi, T.; Etaati, S.; Moradzadeh, A.; Moshtaghi, M.; Nosrati, H.; Brookes, N. J.; Yates, B. F. *Organometallics* **2011**, *30*, 422−432.
(18) The pathway in which the deprotonation occurs first is calculated at the B3LYP/BS2//B3LYP/BS1 level to be 23.6 kcal/mol less favorable than the pathway that starts with the iodine(III) reduction (see Figures S1 and S3 in the Supporting Information).
(19) (a) Koller, R.; Stanek, K.; Stolz, D.; Aardoom, R.; Niedermann, K.; Togni, A. *Angew. Chem., Int. Ed.* **2009**, *48*, 4332−4336. (b) Koller, R.; Huchet, Q.; Battaglia, P.; Welch, J. M.; Togni, A. *Chem. Commun.* **2009**, 5993−5995. (c) Fantasia, S.; Welch, J. M.; Togni, A. *J. Org. Chem.* **2010**, *75*, 1779−1782. (d) Allen, A. E.; MacMillan, D. W. C. *J. Am. Chem. Soc.* **2010**, *132*, 4986−4987. (e) Powers, D. C.; Lee, E.; Ariafard, A.; Sanford, M. S.; Yates, B. F.; Canty, A. J.; Ritter, T. *J. Am. Chem. Soc.* **2012**, *134*, 12002−12009.
(20) The result that Step C is the rate determining step is consistent with the experimental observations; Waser and co-workers concluded that the nucleophilic addition of indole to an electrophilic centre is part of the rate determining step (see ref 3b).
(21) Dapprich, S.; Frenking, G. *J. Phys. Chem.* **1995**, *99*, 9352−9362.
(22) In the CDA analysis, the calculated absolute values for the metal → ligand back-donation (b) and the ligand → metal donation (d) are not very meaningful and in order for the contribution of π-bonding to the metal-ligand interaction to be estimated for comparison, the ratio of these two values (b/d) should be used. For details, see: Lupinetti, A. J.; Jonas, V.; Thiel, W.; Strauss, S. H.; Frenking, G. *Chem.—Eur. J.* **1999**, *5*, 2573−2583.
(23) Lemière, G.; Gandon, V.; Agenet, N; Goddard, J.-P.; de Kozak, A.; Aubert, C.; Fensterbank, L.; Malacria, M. *Angew. Chem., Int. Ed.* **2006**, *45*, 7596−7599.
(24) Robinson, P. S. D.; Khairallah, G. N.; Silva, G.; Lioe, H.; O'Hair, R. A. J. *Angew. Chem., Int. Ed.* **2012**, *51*, 3812−3817.
(25) (a) Ariafard, A.; Tabatabaie, E. S.; Aghmasheh, S.; Najaflo, S.; Yates, B. F. *Inorg. Chem.* **2012**, *51*, 8002−8013. (b) Ariafard, A.; Mahdizadeh Ghohe, N.; Khadem Abbasi, K.; Canty, A. J.; Yates, B. F. *Inorg. Chem.* **2013**, *52*, 707−717.